Journal of Alloys and Compounds 505 (2010) 768–771

Contents lists available at ScienceDirect

Journal of Alloys and Compounds

journal homepage: www.elsevier.com/locate/jallcom

# Preparation, crystallization process and magnetic property of Fe(Co, Ni)ZrB alloy powders

Zhong Hua*, Wanqiu Yu, Yaming Sun, Shuhua Zhao

*College of Physics, Jilin Normal University, No. 1301, Haifeng Street, Tiexi Area, Siping, Jilin, 136000, PR China*

ARTICLE INFO

*Article history:*
Received 5 March 2010
Received in revised form 21 June 2010
Accepted 22 June 2010
Available online 1 July 2010

*Keywords:*
Mechanical alloying
Amorphisation
Scanning electron microscopy

ABSTRACT

Multicomponent $Fe_{70-x}(Co, Ni)_xZr_{10}B_{20}$ ($x = 0, 7, 14, 21, 28$) alloy powders are prepared by mechanical alloying (MA). Co retards the amorphisation of alloy powders while Ni enhances the amorphisation. The crystallization processes of $Fe_{42}Co_{28}Zr_{10}B_{20}$ and $Fe_{42}Ni_{28}Zr_{10}B_{20}$ alloy powders are as amorphous + nanocrystalline → CoFe + remaining amorphous → CoFe + $ZrO_2$ + $Fe_3B$ + unknown phase and amorphous → FeNi + remaining amorphous → FeNi + $ZrFe_2$ + FeB. The coercivity ($\boldsymbol{H_c}$) of $Fe_{42}Co_{28}Zr_{10}B_{20}$ and $Fe_{42}Ni_{28}Zr_{10}B_{20}$ alloy changes with the annealing temperature ($T_a$) as decrease → increase → decrease.



## 1. Introduction

Mechanical alloying (MA) is a solid-state powder processing technique involving repeated welding, fracturing, and rewelding of powder particles in a high-energy ball mill [1]. This technique is an inexpensive method which can be performed to prepare large quantities of nanomaterials and amorphous materials at room temperature using a simple equipment. However, oxygen is always considered as a contamination source for MA experiments, and different kinds of measurements are taken to prevent the oxygen contamination [2].

Extensive studies have been carried out on the mechanical alloying of Fe-based alloys in recent years [3–14]. Magnetic property [3–5], structural characterization [6–11,3] and crystallization behavior [12–14] of Fe-based alloys prepared by MA are investigated. However, the underlying physics of the effects of the content of element on particle size, as well as the annealing temperature ($T_a$) on the coercivity ($\boldsymbol{H_c}$) is still unclear and the detailed investigations are necessary. In this work, $Fe_{70-x}(Co, Ni)_xZr_{10}B_{20}$ ($x = 0$, 7, 14, 21, 28) alloy powders are prepared by MA. The preparation, crystallization process and magnetic property of alloy powders are discussed.

### 2. Experimental

Samples with nominal composition of $Fe_{70-x}(Co, Ni)_xZr_{10}B_{20}$ ($x = 0, 7, 14, 21, 28$) alloy powders were prepared by MA. Premixed powders were sealed in a cylindrical stainless steel vial together with stainless steel balls and milled under an argon atmosphere. Milling procedure was carried out at room temperature by mounting the vial in a GN-2 planetary. The ball-to-powder weight ratio was 40:1. $Fe_{70}Zr_{10}B_{20}$ alloy powders milled for different times and $Fe_{70-x}(Co, Ni)_xZr_{10}B_{20}$ ($x = 7, 14, 21, 28$) alloy powders milled for 50 h were collected. $Fe_{42}Co_{28}Zr_{10}B_{20}$ and $Fe_{42}Ni_{28}Zr_{10}B_{20}$ alloy powders milled for 50 h were annealed at 300, 450, 600 and 750 °C for 1 h at a heating-up rate of 10 °C/min under Ar atmosphere, respectively.

The structure of samples was monitored by X-ray diffraction (XRD, D/max-RA, Cu-Kα, λ = 1.5418 Å). Grain size ($D$) was calculated by Scherrer formula $D = 0.89\lambda/\beta\cos\theta$ ($\beta$ indicates the width of half-height diffraction peak, $\theta$ is Bragg angle, λ is X-ray wavelength, $D$ is grain size). The morphology of samples was characterized by scanning electron microscopy (SEM, S-570). The magnetic property was measured by vibrating sample magnetometer (VSM, Lake Shore M7407). The crystallization temperature was investigated by differential thermal analysis (DTA, PE TG/DTA-6300).

## 3. Results and discussion

XRD patterns of $Fe_{70}Zr_{10}B_{20}$ powders milled for different times are shown in Fig. 1. After 2 h only the peaks of α-Fe phase are observed. After 5 h the characteristic peaks of α-Fe broaden and shift to smaller angles, indicating the refinement of the grain size as well as an increase in the lattice strain [15]. When milling $Fe_{70}Zr_{10}B_{20}$ powders for 50 h, XRD shows a crystal peak superimposes on a broad halo peak, indicating a mixture of nanocrystalline and amorphous.

Fig. 2 shows the XRD patterns of $Fe_{70-x}(Co, Ni)_xZr_{10}B_{20}$ ($x = 0, 7$, 14, 21, 28) powders milled for 50 h. $Fe_{70-x}Co_xZr_{10}B_{20}$ ($x = 7, 14, 21$, 28) powders milled for 50 h are still the mixtures of nanocrystalline and amorphous. However, the peak intensity and angle increase with increasing Co content. The (2 0 0) and (2 1 1) diffraction peaks are also observed. These mean that Co retards the amorphisation of alloy powders. $Fe_{70-x}Ni_xZr_{10}B_{20}$ ($x = 7, 14, 21, 28$) powders milled

* Corresponding author. Tel.: +86 434 3293501; fax: +86 434 3294566.
*E-mail address:* Huazhong196110@163.com (Z. Hua).

0925-8388/$ – see front matter © 2010 Elsevier B.V. All rights reserved.
doi:10.1016/j.jallcom.2010.06.138

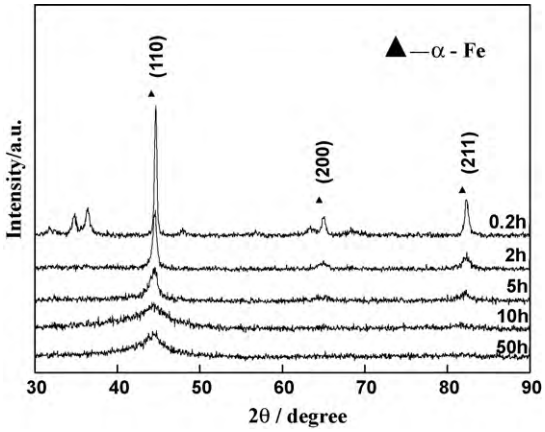


**Fig. 1.** XRD patterns of $Fe_{70}Zr_{10}B_{20}$ powders milled for different times.

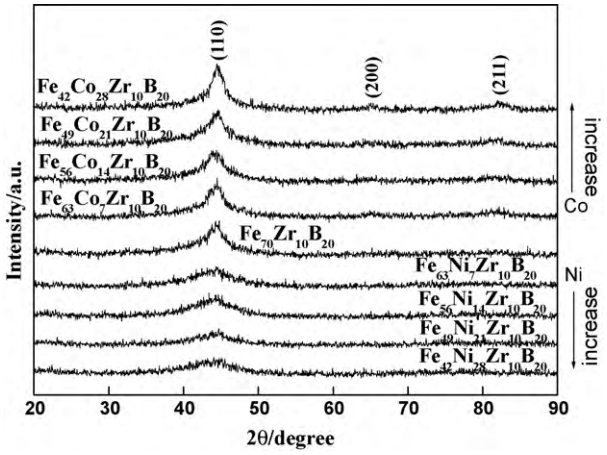


**Fig. 2.** XRD patterns of $Fe_{70-x}(Co, Ni)_xZr_{10}B_{20}$ ($x$ = 0, 7, 14, 21, 28) powders milled for 50 h.

for 50 h form amorphous completely. Ni enhances the amorphisation of alloy powders.

After 50 h $Fe_{70}Zr_{10}B_{20}$ powders experience a characteristic change in particle size and shape as shown in Fig. 3(a) and (b). Morphologies of $Fe_{70-x}(Co, Ni)_xZr_{10}B_{20}$ ($x$ = 7, 14, 21, 28) powders milled for 50 h are shown in Fig. 3(c–j). The particle size of alloy powders is found to be very sensitive to the contents of Co and Ni. Along with the increase of $x$, the powder particle size of $Fe_{70-x}Co_xZr_{10}B_{20}$ ($x$ = 7, 14, 21, 28) decreases while it increases for $Fe_{70-x}Ni_xZr_{10}B_{20}$ ($x$ = 7, 14, 21, 28). The particle size of $Fe_{42}Co_{28}Zr_{10}B_{20}$ and $Fe_{42}Ni_{28}Zr_{10}B_{20}$ powders milled for 50 h is about 5 and 50 μm, respectively. The variation of powder particle size can be ascribed to the welding between elements. Co is less ductile than Fe, and Co substitution for Fe enhances the work hardening and the fracture of powder particles. Ni is more ductile than Fe, and Ni substitution for Fe enhances the welding of powder particles.

XRD patterns of $Fe_{42}Co_{28}Zr_{10}B_{20}$ and $Fe_{42}Ni_{28}Zr_{10}B_{20}$ alloy powders after annealing are shown in Figs. 4 and 5, respectively. $Fe_{42}Co_{28}Zr_{10}B_{20}$ powders milled for 50 h is a mixture of nanocrystalline and amorphous. The diffraction peak intensity of $Fe_{42}Co_{28}Zr_{10}B_{20}$ alloy powders annealed at 300 °C decreases, which may be related to the structure relaxation of the amorphous phase. After annealing at 450 °C, the diffraction peak intensity increases and CoFe phase forms. The crystallization process of $Fe_{42}Co_{28}Zr_{10}B_{20}$ alloy powders is as amorphous + nanocrystalline → CoFe + remaining amorphous → CoFe + $ZrO_2$ + $Fe_3B$ + unknown phase. Grain size of

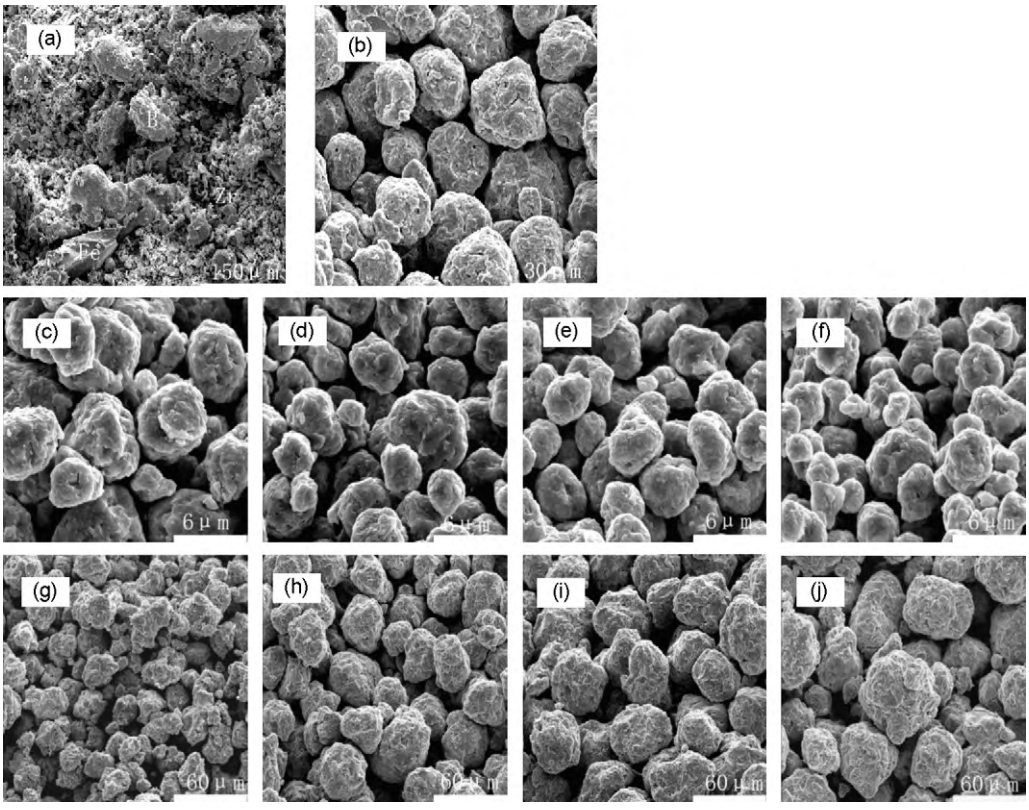


**Fig. 3.** Morphologies of $Fe_{70}Zr_{10}B_{20}$ premixed powders (a) and $Fe_{70-x}(Co, Ni)_xZr_{10}B_{20}$ ($x$ = 0, 7, 14, 21, 28) alloy powders milled for 50 h (b–j). (b) $Fe_{70}Zr_{10}B_{20}$, (c) $Fe_{63}Co_7Zr_{10}B_{20}$, (d) $Fe_{56}Co_{14}Zr_{10}B_{20}$, (e) $Fe_{49}Co_{21}Zr_{10}B_{20}$, (f) $Fe_{42}Co_{28}Zr_{10}B_{20}$, (g) $Fe_{63}Ni_7Zr_{10}B_{20}$, (h) $Fe_{56}Ni_{14}Zr_{10}B_{20}$, (i) $Fe_{49}Ni_{21}Zr_{10}B_{20}$, (j) $Fe_{42}Ni_{28}Zr_{10}B_{20}$.

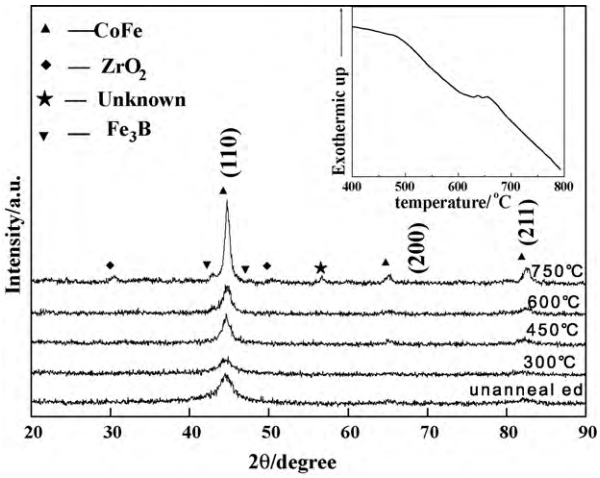


**Fig. 4.** XRD patterns of $Fe_{42}Co_{28}Zr_{10}B_{20}$ powders milled for 50 h and annealed at 300, 450, 600 and 750 °C. The insert shows the DTA curve of $Fe_{42}Co_{28}Zr_{10}B_{20}$ powders milled for 50 h.

$Fe_{42}Co_{28}Zr_{10}B_{20}$ alloy powders annealed at 750 °C is about 105 nm.

$Fe_{42}Ni_{28}Zr_{10}B_{20}$ powders milled for 50 h forms amorphous. After annealing at 300 and 450 °C, the structures of alloy powders are still amorphous. After annealing at 600 °C, the diffraction peak intensity increases and FeNi phase forms. The crystallization process of $Fe_{42}Ni_{28}Zr_{10}B_{20}$ alloy powders is as amorphous → FeNi + remaining amorphous → FeNi + $ZrFe_2$ + FeB, which is different from that found by Liu et al. [10]. This may be due to the different annealing conditions. Grain size of $Fe_{42}Ni_{28}Zr_{10}B_{20}$ alloy powders annealed at 750 °C is about 100 nm.

XRD pattern of $Fe_{42}Co_{28}Zr_{10}B_{20}$ alloy powders annealed at 750 °C shows the precipitation of $ZrO_2$ and the precipitation is not observed in the $Fe_{42}Ni_{28}Zr_{10}B_{20}$ alloy powders. It is possible that the $O_2$ content in as-milled $Fe_{42}Co_{28}Zr_{10}B_{20}$ alloy powders is higher than that in as-milled $Fe_{42}Ni_{28}Zr_{10}B_{20}$ alloy powders.

Fig. 6 shows the coercivity ($\boldsymbol{H_c}$) of $Fe_{42}Co_{28}Zr_{10}B_{20}$ and $Fe_{42}Ni_{28}Zr_{10}B_{20}$ alloy powders as a function of annealing temperature ($T_a$). $\boldsymbol{H_c}$ of $Fe_{42}Co_{28}Zr_{10}B_{20}$ alloy powders is larger than that of $Fe_{42}Ni_{28}Zr_{10}B_{20}$ alloy powders at every annealing stage, which is related to the $O_2$ content of alloy powders.

$\boldsymbol{H_c}$ of $Fe_{42}Co_{28}Zr_{10}B_{20}$ and $Fe_{42}Ni_{28}Zr_{10}B_{20}$ alloy powders both show the change as decrease → increase → decrease. The decrease

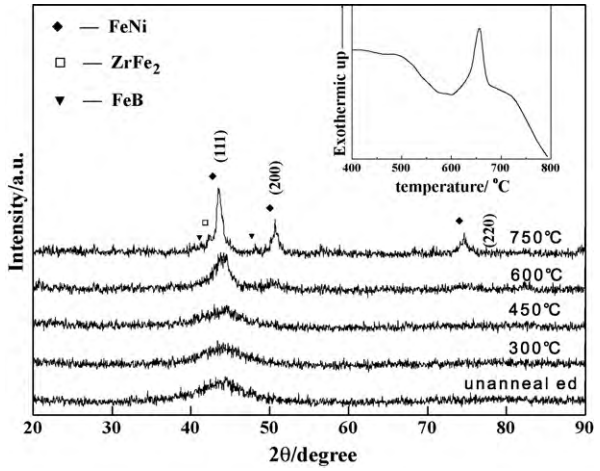


**Fig. 5.** XRD patterns of $Fe_{42}Ni_{28}Zr_{10}B_{20}$ powders milled for 50 h and annealed at 300, 450, 600 and 750 °C. The insert shows the DTA curve of $Fe_{42}Ni_{28}Zr_{10}B_{20}$ powders milled for 50 h.

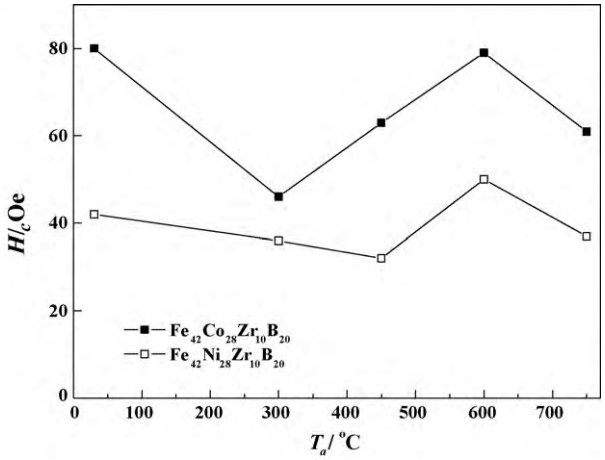


**Fig. 6.** Coercivity ($\boldsymbol{H_c}$) of $Fe_{42}Co_{28}Zr_{10}B_{20}$ and $Fe_{42}Ni_{28}Zr_{10}B_{20}$ alloy powders as a function of annealing temperature ($T_a$).

of $\boldsymbol{H_c}$ in the initial annealing stage is ascribed to the structure relaxation of amorphous phase. $Fe_{42}Co_{28}Zr_{10}B_{20}$ and $Fe_{42}Ni_{28}Zr_{10}B_{20}$ alloy powders show the different annealing temperature for structure relaxation. $\boldsymbol{H_c}$ of $Fe_{42}Co_{28}Zr_{10}B_{20}$ and $Fe_{42}Ni_{28}Zr_{10}B_{20}$ alloy powders decreases to the minimum value at 300 and 450 °C, respectively. Nanocrystallines precipitate and a great deal of interfaces form with increasing annealing temperature. The continuous increase of interfaces hinders the movement of magnetic domain walls, causing the rapid increase of $\boldsymbol{H_c}$ [16]. Grain sizes of $Fe_{42}Co_{28}Zr_{10}B_{20}$ and $Fe_{42}Ni_{28}Zr_{10}B_{20}$ alloy powders annealed at 750 °C are very large, which meets the classical rule that $\boldsymbol{H_c}$ is in inverse ratio to $D$ [17]. $Fe_{42}Co_{28}Zr_{10}B_{20}$ and $Fe_{42}Ni_{28}Zr_{10}B_{20}$ alloy powders show the decreased $\boldsymbol{H_c}$ when annealed at 750 °C.

## 4. Conclusions

(1) $Fe_{70-x}Co_xZr_{10}B_{20}$ ($x$ = 7, 14, 21, 28) alloy powders milled for 50 h are the mixtures of nanocrystalline and amorphous. XRD diffraction peak intensity and angle increase with increasing Co content. The (2 0 0) and (2 1 1) diffraction peaks are observed. $Fe_{70-x}Ni_xZr_{10}B_{20}$ ($x$ = 7, 14, 21, 28) alloy powders milled for 50 h form amorphous phase completely.

(2) Along with the increase of $x$, the powder particle size of $Fe_{70-x}Co_xZr_{10}B_{20}$ ($x$ = 7, 14, 21, 28) decreases while it increases for $Fe_{70-x}Ni_xZr_{10}B_{20}$ ($x$ = 7, 14, 21, 28). The variation in powder particle size can be ascribed to the welding between elements.

(3) The crystallization processes of $Fe_{42}Co_{28}Zr_{10}B_{20}$ and $Fe_{42}Ni_{28}Zr_{10}B_{20}$ alloy powders are as amorphous + nanocrystalline → CoFe + remaining amorphous → CoFe + $ZrO_2$ + $Fe_3B$ + unknown phase and amorphous → FeNi + remaining amorphous → FeNi + $ZrFe_2$ + FeB.

(4) The coercivity ($\boldsymbol{H_c}$) of $Fe_{42}Co_{28}Zr_{10}B_{20}$ and $Fe_{42}Ni_{28}Zr_{10}B_{20}$ alloy powders as a function of annealing temperature both show the change as decrease → increase → decrease. The decrease of $\boldsymbol{H_c}$ in the initial annealing stage is ascribed to the structure relaxation of amorphous phase. The increase of $\boldsymbol{H_c}$ is related to magnetic domain wall pinning. Grain size ($D$) of alloy powders annealed at 750 °C meets the classical rule, and $\boldsymbol{H_c}$ of alloy powders annealed at 750 °C decreases at last.

## Acknowledgement

This work was funded by Science and Technology Development Project of Jilin Province (No. 20082112).

## References


[1] C. Suryanarayana, Prog. Mater. Sci. 46 (2001) 1–184.
[2] C.Q. Zhang, Z.H. Zhang, Z. Qi, Y.X. Qi, J.Y. Zhang, X.F. Bian, J. Non-Cryst. Solids 354 (2008) 3812–3822.
[3] B. Bhoi, V. Srinivas, V. Singh, J. Alloys Compd. 496 (2010) 423–428.
[4] S. Alleg, M. Ibrir, N.E. Fenineche, S. Azzaza, R. Bensalem, J.J. Suñol, J. Alloys Compd. 494 (2010) 109–115.
[5] A.F. Cabrera, C.E. Rodríguez Torres, P. Mendoza Zélis, M. Fernández Van Raap, L.M. Socolovsky, G. Pasquevich, F.H. Sánchez, Phys. B 354 (2004) 129–132.
[6] J.J. Suñol, J.M. Güell, J. Bonastre, S. Alleg, J. Alloys Compd. 483 (2009) 604–607.
[7] J.S. Blázquez, J.J. Ipus, M. Millán, V. Franco, A. Conde, D. Oleszak, T. Kulik, J. Alloys Compd. 469 (2009) 169–178.
[8] J.J. Suñol, A. González, J. Bonastre, M.T. Clavaguera-Mora, B. Arcondo, J. Alloys Compd. 434–435 (2007) 415–419.
[9] A. Grabias, M. Kopcewicz, D. Oleszak, J. Alloys Compd. 339 (2002) 221–229.
[10] Y.J. Liu, I.T.H. Chang, P. Bowen, Mater. Sci. Eng. A 304–306 (2001) 389–393.
[11] Z. Hua, Y.M. Sun, W.Q. Yu, M.B. Wei, L.H. Liu, J. Alloys Compd. 477 (2009) 529–531.
[12] B. Movahedi, M.H. Enayati, C.C. Wong, Mater. Lett. 64 (2010) 1055–1058.
[13] Md. Sultan Mahmud, M.A. Hakim, S. Manjura Hoque, S.S. Sikder, A.K. Gain, Nordblad Per, AIP Conf. Proc. 1003 (2008) 55–57.
[14] Y.J. Liu, I.T.H. Chang, Mater. Sci. Eng. A 325 (2002) 25–30.
[15] E. Hellstern, H.J. Fecht, Z. Fu, W.L. Johnson, J. Appl. Phys. 65 (1989) 305–310.
[16] Y. Hu, L. Liu, K.C. Chan, M.X. Pan, W.H. Wang, Mater. Lett. 60 (2006) 1080–1084.
[17] G. Herzer, J. Magn. Magn. Mater. 112 (1992) 258–262.